Quantum Solvent and Solute Effects in the Infrared Vibrational Echo†

Ryo Akiyama and Roger F. Loring*

Department of Chemistry and Chemical Biology, Baker Laboratory, Cornell University, Ithaca, New York 14853

Received: August 20, 2002; In Final Form: November 8, 2002

The infrared echo measurement distinguishes among vibrational line broadening processes according to their time scales. Rigorous computation of the echo signal for a realistic model requires quantum dynamical calculations for large anharmonic systems. The challenges posed by such calculations motivate the use of classical mechanical or semiclassical approximations. The application of such approaches to compute the vibrational echo signal depends on the nature and magnitude of quantum effects on the echo observable. We quantify these effects for a generic model of an anharmonic oscillator coupled to a harmonic solvent in the regimes of classical solvent and classical solute, classical solvent and quantum solute, and quantum solvent and quantum solute.

Introduction

Coherent infrared spectroscopies represent analogs of multiple pulse magnetic resonance techniques.[1−9] The vibrational echo, the analog of the spin echo, probes the loss of phase coherence of a vibrational degree of freedom resulting from interactions with its environment.[2,3,8,9] These dephasing dynamics encompass both resonant and nonresonant energy transfer processes, as well as adiabatic pure dephasing processes, in which phase coherence is lost without transfer of vibrational energy. Two and three pulse vibrational echo measurements have been applied to probe configurational dynamics in biomolecules and other liquid state systems.[2,3,8,9] Complete interpretation of such measurements requires the modeling of the nonlinear vibrational response of large anharmonic systems with an atomic level of detail.[8−13] Since full quantum dynamical calculations for such systems are not feasible, practical calculations must make use of classical mechanical[14−16] or semiclassical treatments. It is therefore necessary to analyze the nonlinear response of model anharmonic systems[17,18] that are sufficiently simple to permit both quantum and classical treatments in order to understand the nature of quantum mechanical effects, and to map out the regimes of applicability of less than fully quantum mechanical dynamical approaches.

We have previously computed the vibrational echo signal for such a model: a Morse oscillator coupled to a harmonic solvent with an interaction that is bilinear in solute and solvent coordinates.[17] We assumed a separation of time scales between a high-frequency solute and a low-frequency solvent, so that only pure dephasing processes were included. In that treatment, the solvent was represented in the classical mechanical limit, and solute parameters were varied from a fully classical regime to a completely quantum mechanical one. The theory of ref 17 was shown to be quantitatively accurate in the fully classical limit by comparison with numerically exact classical mechanical calculations[15] of the vibrational echo. We demonstrated[17] that purely classical mechanical echo calculations are qualitatively correct for a high-frequency and nominally quantum mechanical solute coupled to a classical solvent. This work elucidated the effects of quantum mechanical solute dynamics on the echo observable. In the present work, we investigate the role of quantum mechanical solvent dynamics on the echo signal, by generalizing the treatment of ref 17 to compute vibrational echoes for a quantum anharmonic oscillator interacting with a quantum solvent.

Vibrational Echo from a Solvated Oscillator

We treat a Morse oscillator[19] linearly coupled to a harmonic solvent with the Hamiltonian,

$$\hat{H} = \frac{\hat{p}^2}{2m_0} + \frac{\hbar\omega_0^{\,2}}{2\Delta}[1 - \exp(-\sqrt{m_0\Delta/\hbar}\,\hat{q})]^2 + \frac{1}{2}\sum_{\nu=1}^{N}\left\{\frac{\hat{p}_\nu^{\,2}}{m_\nu} + m_\nu\left(\omega_\nu\hat{q}_\nu - \frac{c_\nu\hat{q}}{m_\nu\omega_\nu}\right)^2\right\} \quad (1)$$

Momentum, coordinate, and mass are denoted $\hat{p}$, $\hat{q}$, and m_0 for the solute, and $\hat{p}_\nu$, $\hat{q}_\nu$, and m_ν for solvent degrees of freedom. The conventional parameters of the Morse potential have been reexpressed in terms of ω_0, the harmonic frequency,[17] and Δ, the difference between the $n \rightarrow n+1$ and $n+1 \rightarrow n+2$ transition frequencies of an unsolvated Morse oscillator. In ref 17, we developed an analytical theory for the vibrational echo of this model, based on four assumptions. First, the solute frequency is higher than relevant solvent frequencies, $\omega_0 \gg \omega_\nu$. Within this assumption, the echo is governed by adiabatic, pure dephasing processes, and the contributions of resonant energy transfer between solute and solvent are negligible. Second, the adiabatic solvent Hamiltonian resulting from the first assumption is evaluated to lowest order in solute−solvent coupling c_ν. Third, the solute anharmonicity is assumed to be small, $\Delta \ll \omega_0$. Fourth, the solvent is taken to be classical mechanical; the thermal time scale $\beta\hbar$, with $\beta = 1/k_BT$, is assumed to be small compared to any relevant solvent time scale. Here, we generalize the development of ref 17 by computing the third-order response function for the model of eq 1 retaining the first three assumptions just described, but discarding the fourth assumption of a classical mechanical solvent.

† Part of the special issue "A. C. Albrecht Memorial Issue".

10.1021/jp021906p CCC: $25.00
Published on Web 01/04/2003

We briefly summarize the generalization of the vibrational echo calculation in ref 17. To lowest order in solute−solvent coupling, the adiabatic solvent Hamiltonian associated with the nth solute excited state is

$$\hat{H}_n = \epsilon_n \hat{I} + \frac{1}{2}\sum_{\nu=1}^{N}\left\{\frac{\hat{p}_\nu^{\,2}}{m_\nu} + m_\nu\omega_\nu^{\,2}\hat{q}_\nu^{\,2} - 2c_\nu\hat{q}_\nu\langle n|\,\hat{q}|\,n\rangle\right\} \quad (2)$$

$$\epsilon_n = \hbar\omega_0(n+1/2) - \hbar\frac{\Delta}{2}(n+1/2)^2 \quad (3)$$

The identity operator in the space of solvent states is denoted $\hat{I}$, and $|\,n\rangle$ represents an energy eigenstate of the isolated solute. The electric polarization $P(t)$ generating the signal in a third-order nonlinear optical measurement such as the vibrational echo may be computed[17,20] from the third-order response function,[20−24] $R^{(3)}(t_1,t_2,t_3)$, in which the t_j denote elapsed times between successive interactions with the classical electric field $E(t)$,

$$P(t) = \int_0^\infty dt_1 \int_0^\infty dt_2 \int_0^\infty dt_3\, E(t-t_1-t_2-t_3)E(t-t_2-t_3)E(t-t_3)R^{(3)}(t_1,t_2,t_3) \quad (4)$$

The signal in a two-pulse echo measurement in the limit of impulsive excitation may be computed from this response function with $t_1 = \tau$, the delay time between excitation pulses, $t_2 = 0$, and $t_3 = t - \tau$, with t the detection time. This quantity is related to equilibrium correlation functions of the dipole operator $\hat{\mu}$ by[20]

$$R^{(3)}(\tau,0,t-\tau) \equiv 2\mathrm{Im}[2R_\mathrm{I} + R_\mathrm{II} + R_\mathrm{III}] \quad (5)$$

$$R_\mathrm{I} = \hbar^{-3}\langle\hat{\mu}(0)\hat{\mu}(\tau)\hat{\mu}(t)\hat{\mu}(\tau)\rangle \quad (6)$$

$$R_\mathrm{II} = \hbar^{-3}\langle\hat{\mu}(t)\hat{\mu}(\tau)\hat{\mu}(\tau)\hat{\mu}(0)\rangle \quad (7)$$

$$R_\mathrm{III} = \hbar^{-3}\langle\hat{\mu}(\tau)\hat{\mu}(\tau)\hat{\mu}(t)\hat{\mu}(0)\rangle \quad (8)$$

with Im denoting the imaginary part of a complex number. Angle brackets denote an average over the thermal density matrix.

Within the adiabatic approximation of eq 2, the thermal average over the harmonic solvent degrees of freedom in eqs 6−8 may be performed analytically.[17] With an additional assumption of weak anharmonicity, as detailed in eq 23 of ref 17, the relevant dipole correlation functions are given by

$$R_\mathrm{I} = \left\langle\sum_{mlk}\mu_{nm}\mu_{ml}\mu_{lk}\mu_{kn}\exp[i\omega_0 t(l-k)]\exp[-i\omega_0\tau(l-k-m+n)]\exp\left\{i\frac{\Delta}{2}t[k(k+1)-l(l+1)]\right\}\times\exp\left\{i\frac{\Delta}{2}\tau[n(n+1)-m(m+1)+l(l+1)-k(k+1)]\right\}\exp\{-(n-m)(n-m+l-k)\Gamma^*(\tau)-(n-m)(k-l)\Gamma^*(t)-(l-k)[(l-m)\Gamma^*(t-\tau)+(n-k)\Gamma(t-\tau)]\}\right\rangle_n \quad (9)$$

$$R_\mathrm{II} = \left\langle\sum_{mlk}\mu_{nm}\mu_{ml}\mu_{lk}\mu_{kn}\exp[i\omega_0 t(n-m)]\exp[i\omega_0\tau(m-k)]\times\exp\left\{i\frac{\Delta}{2}t[m(m+1)-n(n+1)]\right\}\exp\left\{i\frac{\Delta}{2}\tau[k(k+1)-m(m+1)]\right\}\exp\{-(n-k)(m-k)\Gamma(\tau)-(n-m)(n-k)\Gamma(t)-(n-m)(k-m)\Gamma(t-\tau)\}\right\rangle_n \quad (10)$$

$$R_\mathrm{III} = \left\langle\sum_{mlk}\mu_{nm}\mu_{ml}\mu_{lk}\mu_{kn}\exp[i\omega_0 t(l-k)]\exp[i\omega_0\tau(n-l)]\times\exp\left\{i\frac{\Delta}{2}t[k(k+1)-l(l+1)]\right\}\exp\left\{i\frac{\Delta}{2}\tau[l(l+1)-n(n+1)]\right\}\exp\{-(n-k)(n-l)\Gamma(\tau)-(n-k)(l-k)\Gamma(t)-(n-l)(k-l)\Gamma^*(t-\tau)\}\right\rangle_n \quad (11)$$

The thermal average of a quantity b_n over bound states of the isolated solute is given by

$$\langle b_n\rangle_n \equiv \frac{\sum_{n=0}^{n_\mathrm{max}} b_n\exp(-\beta\epsilon_n)}{\sum_{n=0}^{n_\mathrm{max}}\exp(-\beta\epsilon_n)} \quad (12)$$

The index n_max is the quantum number of the highest energy bound state of the Morse oscillator. The complex-valued solvent relaxation kernel $\Gamma(t)$ is defined by

$$\Gamma(t) = \frac{F^2\hbar\beta}{4m_0}\int_0^t d\tau\left[(t-\tau)\zeta(\tau) + \frac{i}{2}[\eta(\tau)-\eta(0)]\right] \quad (13)$$

$$F = \frac{3}{\omega_0}\sqrt{\Delta/\hbar\beta} \quad (14)$$

$$\eta(t) = \sum_{\nu=1}^{N}\frac{c_\nu^{\,2}}{m_\nu\omega_\nu^{\,2}}\cos(\omega_\nu t) \quad (15)$$

$$\zeta(t) = \frac{1}{\pi}\int_0^\infty d\omega\;\omega\cos(\omega t)\coth\left(\frac{\beta\hbar\omega}{2}\right)\hat{\eta}(\omega) \quad (16)$$

The classical mechanical solvent friction kernel[25] $\eta(t)$ is defined in eq 15 and a dimensionless, temperature-dependent solute anharmonicity F is given in eq 14. Equation 16 contains the cosine transform of the friction kernel, $\hat{\eta}(\omega) = \int_0^\infty dt\cos(\omega t)\,\eta(t)$. Replacement of the relaxation kernel $\Gamma(t)$ with its real-valued $\hbar\to 0$ limit yields the approximation to the response function employed in ref 17. We evaluate the dipole matrix elements in eqs 9−11 by taking the dipole operator to be proportional to the coordinate, $\hat{\mu} = e_0\hat{q}$. These matrix elements are evaluated in the harmonic oscillator limit, in keeping with the assumption of low anharmonicity.[17]

The signal $S(\tau)$ in the two-pulse vibrational echo in the limit of impulsive excitation is related to a complex-valued temporally

slowly varying electric polarization amplitude[20] $\tilde{P}(t,\tau)$ by

$$S(\tau) \equiv \int_{\tau}^{\infty} \mathrm{d}t\, |\tilde{P}(t,\tau)|^2 \tag{17}$$

This polarization is connected to the response function by $\tilde{P}(t,\tau) = A^3 \exp[i\Omega(t-2\tau)]R^{(3)}(\tau,0,t-\tau)$, with A representing the time-integrated electric field amplitude and Ω denoting the central frequency of an excitation pulse. This expression is evaluated by retaining terms that oscillate in t at $\Omega - \omega_0$ and neglecting terms that oscillate in t at $\Omega + \omega_0$. Here, we set $\Omega = \omega_0$. For the response function in eqs 9−11, this polarization amplitude takes the form

$$\tilde{P}(t,\tau) = \left[\frac{A^3 e_0{}^4}{4m_0{}^2\omega_0{}^2\hbar}\right]\{\Lambda_{\mathrm{re}}[X_{\mathrm{re}}'' + Y_{\mathrm{re}}'' + i(X_{\mathrm{re}}' - Y_{\mathrm{re}}')] + \Lambda_{nr}e^{-2i\omega_0\tau}[X_{nr}'' + Y_{nr}'' + i(X_{nr}' - Y_{nr}')]\} \tag{18}$$

analogous to eq 40 of ref 17. The contribution to the echo decay from solvent dynamics is contained within the *rephasing* and *nonrephasing* solvent relaxation functions,[20] $\Lambda_{\mathrm{re}}(t,\tau)$ and $\Lambda_{nr}(t)$, while the solute contribution to the echo dynamics is contained within the complex-valued functions $X_{\mathrm{re}}(t,\tau)$, $Y_{\mathrm{re}}(t,\tau)$, $X_{nr}(t,\tau)$, and $Y_{nr}(t,\tau)$. The real and imaginary parts of a complex-valued quantity are defined by $X = X' + iX''$.

The solvent relaxation functions are given by

$$\Lambda_{\mathrm{re}}(t,\tau) = \exp[-2\Gamma'(\tau) - 2\Gamma'(t-\tau) + \Gamma'(t)] \tag{19}$$

$$\Lambda_{nr}(t) = \exp[-\Gamma'(t)] \tag{20}$$

The rephasing relaxation function is so named because in the short-time limit of $\Gamma'(t) \propto t^2$, $\Lambda_{\mathrm{re}}(t,\tau)$ is peaked at $t = 2\tau$, representing the rephasing of the macroscopic polarization associated with a conventional photon echo.[20,26] The factors carrying the effects of solute dynamics on the echo signal are given by

$$X_{\mathrm{re}}(t,\tau) = 2N_2{}^*(\theta)[e^{2i\Gamma''(\tau)-i\Gamma''(t)} - 1] + [N_2{}^*(\theta) + N_1{}^*(\theta)][e^{i\Delta\tau}e^{i[-2\Gamma''(\tau)-2\Gamma''(t-\tau)+\Gamma''(t)]} - 1] + [N_2{}^*(\theta) + 3N_1{}^*(\theta) + 2N_0{}^*(\theta)][e^{i\Delta(3\tau-2t)}e^{i[-2\Gamma''(\tau)+\Gamma''(t)+2\Gamma''(t-\tau)]} - 1] \tag{21}$$

$$Y_{\mathrm{re}}(t,\tau) = 2[N_2(\theta) + 2N_1(\theta) + N_0(\theta)][e^{i\Delta(t-2\tau)}e^{i[2\Gamma''(\tau)-\Gamma''(t)]} - 1] + [N_2(\theta) + N_1(\theta)][e^{i\Delta(t-\tau)}e^{i[-2\Gamma''(\tau)-2\Gamma''(t-\tau)+\Gamma''(t)]} - 1] + [N_2(\theta) - N_1(\theta)][e^{-i\Delta(t-\tau)}e^{i[-2\Gamma''(\tau)+2\Gamma''(t-\tau)+\Gamma''(t)]} - 1] \tag{22}$$

$$\theta = \Delta(t - 2\tau) \tag{23}$$

$$X_{nr}(t,\tau) = [N_2{}^*(\Delta t) + 3N_1{}^*(\Delta t) + 2N_0{}^*(\Delta t)] \times [e^{i\Delta(\tau-2t)}e^{i[\Gamma''(t)+2\Gamma''(t-\tau)]} - 1] + [N_2{}^*(\Delta t) + N_1{}^*(\Delta t)] \times [e^{-i\Delta\tau}e^{i[\Gamma''(t)-2\Gamma''(t-\tau)]} - 1] + 2N_2{}^*(\Delta t)[e^{-i\Gamma''(t)} - 1] \tag{24}$$

$$Y_{nr}(t,\tau) = [N_2(\Delta t) - N_1(\Delta t)][e^{-i\Delta(t-\tau)}e^{i[\Gamma''(t)+2\Gamma''(t-\tau)]} - 1] + [N_2(\Delta t) + N_1(\Delta t)][e^{i\Delta(t-\tau)}e^{i[\Gamma''(t)-2\Gamma''(t-\tau)]} - 1] + 2[N_2(\Delta t) + 2N_1(\Delta t) + N_0(\Delta t)][e^{i\Delta t}e^{-i\Gamma''(t)} - 1] \tag{25}$$

$$N_j(x) \equiv \langle n^j e^{inx}\rangle_n \tag{26}$$

The complex-valued functions N_j contribute oscillations in t and τ at multiples of the solute anharmonic frequency Δ to the electric polarization. For the calculations presented in the next section, N_j is evaluated from eqs 12 and 26 in a harmonic approximation in which $n_{\max} \rightarrow \infty$ and $\epsilon_n \rightarrow n\hbar\omega_0$. This approximation yields analytic expressions for N_j and is consistent with the low anharmonicity approximation made elsewhere.[17] Complete specification of the model of eq 1 requires identification of the friction kernel[25] $\eta(t)$. We consider the limit of a continuum solvent with friction kernel appropriate to an Ohmic density of states with an exponential cutoff in frequency,[27]

$$\eta(t) = \frac{2\eta}{\pi}\frac{\lambda}{\lambda^2 + t^2} \tag{27}$$

For this choice, $\hat{\eta}(\omega) = \eta \exp(-\lambda\omega)$. The solvent time scale λ is a measure of the width of the distribution of solvent frequencies. The classical solvent limit of ref 17 is recovered by taking the $\beta\hbar \ll \lambda$ limit of eq 16 in which $\zeta(t)$ is proportional to the classical friction, $\zeta(t) \rightarrow 2\eta(t)/\beta\hbar$. Substitution of this result into eq 13 results in a real-valued $\Gamma(t)$ that is independent of $\hbar$. The calculations of the echo signal in ref 17 were performed using eqs 17 and 18 with $\Gamma'(t)$ in eqs 19 and 20 replaced by its $\hbar \rightarrow 0$ limit, and $\Gamma''(t)$ in eqs 21, 22, 24, and 25 set to zero. In the next section, we present calculations of $S(\tau)$ using the full quantum expression for $\Gamma(t)$ in eq 13.

Numerical Results

The importance of quantum mechanics to the vibrational echo signal for the model specified by eqs 1 and 27 is determined by the relative magnitudes of three time scales: $\beta\hbar$, the quantum mechanical thermal time scale; λ, the time scale in eq 27 that determines the width of the distribution of solvent frequencies; and $\omega_0{}^{-1}$, the inverse solute frequency. The theory of the previous section[17] is based on the assumption of a separation of time scales between solute and solvent, namely, that $\omega_0{}^{-1} \ll \lambda$. It is therefore valid in three limiting regimes: classical solute and classical solvent ($\beta\hbar \ll \omega_0{}^{-1} \ll \lambda$), quantum solute and classical solvent ($\omega_0{}^{-1} \ll \beta\hbar \ll \lambda$), and quantum solute and quantum solvent ($\omega_0{}^{-1} \ll \lambda \ll \beta\hbar$). The first two regimes were treated in ref 17. As discussed there,[17] the limit of motional narrowing or rapid solvent-induced fluctuations of the spectroscopic transition frequency[20,26,28] is attained for $\lambda \ll T_2$, with $T_2 = 4m_0/(F^2\eta)$, the pure dephasing time.[27,29,30] This quantity, which represents the coherence decay time of a quantum solute interacting with a low-frequency solvent, is independent of $\hbar$, and hence should be regarded as classical mechanical.[15,30] For a classical solvent ($\lambda \gg \beta\hbar$) in the limit $\lambda \ll T_2$, the decay kernel in eq 13 is linear in time, $\Gamma(t) \rightarrow t/T_2$, and the echo signal decays as a free induction decay, $\ln[S(\tau)] \propto -2\tau/T_2$. The opposite limit, $\lambda \gg T_2$, represents the approach to static line broadening. In ref 17, we compared echo calculations for classical and quantum solutes with classical solvents in both the motional narrowing and slow solvent limits. We found that quantum solute effects, the deviations of a quantum calculation of $S(\tau)$ from a fully classical one, become more pronounced as the time scale of the solvent increases.[17]

Calculations of the vibrational echo signal for a classical solvent and classical and quantum solutes are shown in Figure 1, in which the solute anharmonicity is $F = 0.45$, the friction is $\eta = m_0\omega_0$, and the solvent time scale is $\lambda = 30\omega_0{}^{-1}$. This value of F corresponds to significant solute anharmonicity. For example, the dimensionless bond anharmonicity of the CO molecule, a chromophore in vibrational echo measurements,[2,8] at room temperature is $F \approx 0.1$. This value of η corresponds to moderate solute−solvent coupling.[16] We verified by comparison

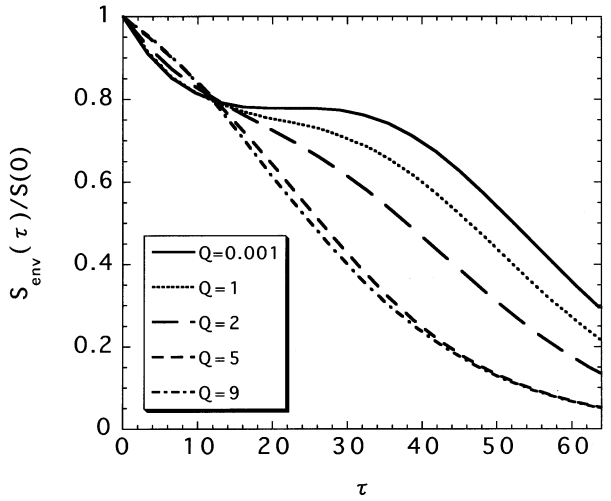

Figure 1. Quantum solute effects in the vibrational echo signal $S(\tau)$ are shown for a Morse oscillator coupled to a harmonic solvent, with dimensionless anharmonicity $F = 0.45$, friction coefficient $\eta = m_0\omega_0$ and solvent time scale $\lambda = 30\omega_0^{-1}$. The classical limit, $Q = 0.001$, is shown by the solid curve, and the importance of quantum solute dynamics increases as Q is raised to $Q = 1$ (dots), $Q = 2$ (long dash), $Q = 5$ (short dash), and $Q = 9$ (dash−dot). The delay time τ is expressed in units of ω_0^{-1}.

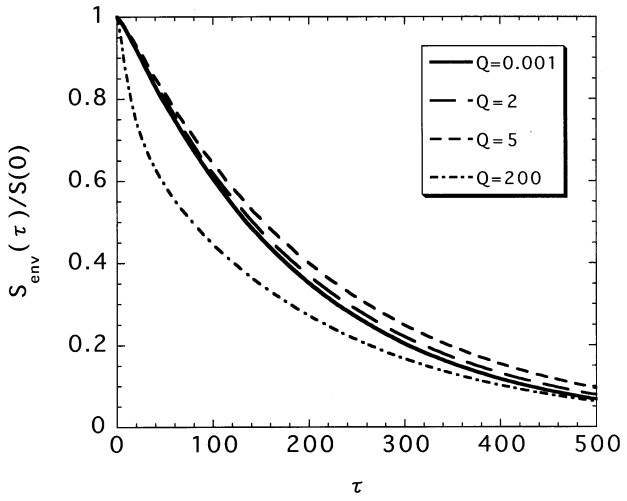

Figure 2. Quantum solute and solvent effects in the vibrational echo signal $S(\tau)$ are shown for $F = 0.1$, $\lambda = 6\omega_0^{-1}$, and $\eta = m_0\omega_0$ for $Q = 0.001$ (classical limit, solid curve), $Q = 2$ (long dash), $Q = 5$ (short dash), and $Q = 200$ (dash−dot).

to numerical simulation of the classical vibrational echo[15,16] that the theory is accurate for these parameter values in the classical limit.[17] The value of the classical dephasing time for these parameters is $T_2 = 19.8\omega_0^{-1}$. The value $\lambda = 30\omega_0^{-1}$ was chosen so that $\lambda > T_2$, which signifies that this system corresponds to line broadening intermediate between the limits of static line broadening and motional narrowing. As defined in eq 17, the echo signal $S(\tau)$ oscillates at a frequency close to the solute frequency ω_0, as a consequence of the assumption of impulsive excitation by laser pulses of duration short compared to the solute vibrational period. Figure 1 and the subsequent figures show the normalized envelope of this oscillatory decay, $S_{env}(\tau)/S(0)$, defined by interpolating between the maxima of these rapid oscillations. In all figures, the τ axis is scaled by the solute frequency ω_0. The importance of quantum effects is controlled by the value of $Q \equiv \beta\hbar\omega_0$, which is varied from $Q = 0.001$ (solid) to $Q = 1$ (dots), $Q = 2$(long dash), $Q = 5$(short dash), and $Q = 9$ (dot−dash). The curve with $Q = 0.001$ represents the complete classical limit $Q \rightarrow 0$, in which both solute and solvent are treated classically. Since both the dimensionless anharmonicity F and Q depend on temperature, varying Q at fixed F as in Figure 1 does not correspond to changing the temperature for a system with fixed Hamiltonian parameters. Temperature variation at fixed parameters would result from changing Q and F at fixed F^2Q. We choose to vary Q for fixed F, because comparing a calculation at nonzero Q to one in the $Q \rightarrow 0$ limit for the same value of F corresponds to comparing a quantum calculation at specified temperature and model parameters to a classical calculation for the same model at that temperature. The echo signal in the classical limit displays decays at short and at longer times separated by a plateau, as is characteristic of the classical echo for a system approaching the limit of static line broadening.[16,17] Increasing the effect of quantum mechanics by increasing Q causes the early decay to become slower while the decay at longer times becomes more rapid. Increasing Q from $Q = 5$ to $Q = 9$ has little effect on the echo decay, because in this regime $\lambda\omega_0 > Q > 1$. The value of Q is sufficiently large that the solute is fully quantum mechanical, but is still small enough that the low-frequency solvent is completely classical mechanical. In principle, for sufficiently large Q values, $Q \gg \lambda\omega_0$, the echo signal will display the effects of quantum solvent dynamics. This limit is not attainable for the parameters of Figure 1, because increasing Q at fixed F corresponds to decreasing the number of bound states of the Morse oscillator.[19] To support at least three bound states, the minimum number of states assumed in the theoretical development of the previous section, $Q < 18/(7F^2)$. This constraint does not permit access to the quantum solvent regime, $Q > \lambda\omega_0$, for the values of λ and F employed in Figure 1.

Examination of quantum solvent effects in the regime $Q > \lambda\omega_0$ requires decreasing the dimensionless anharmonicity F and the solvent time scale λ from the values employed in Figure 1, which brings the system closer to the limit of motional narrowing. Figure 2 shows the echo signal for $F = 0.1$, $\lambda = 6\omega_0^{-1}$, and $\eta = m_0\omega_0$ with $Q = 0.001$ (solid), $Q = 2$ (long dash), $Q = 5$ (short dash), and $Q = 200$ (dot−dash). The classical dephasing time is $T_2 = 400\omega_0^{-1}$, so that the system is indeed approaching the limit of motional narrowing with $T_2 \gg \lambda$. As Q is increased from the classical limit shown by the solid curve, the influence of quantum effects on the solute dynamics increases, and the decay slows as also evident in the short-time dynamics of Figure 1. However, as Q becomes comparable in magnitude to $\lambda\omega_0$, quantum solvent effects become apparent and the decay becomes faster with increasing Q, as evident from the comparison of the $Q = 5$ and $Q = 200$ calculations in Figure 2. Quantum solvent effects are embodied in the deviations of $\Gamma'(t)$ in eq 13 from its finite $\hbar \rightarrow 0$ limit and in $\Gamma''(t)$, which vanishes as $\hbar \rightarrow 0$. Γ'' contributes to a frequency shift in the oscillations of $S(\tau)$, while Γ' contributes to the τ dependence of $S_{env}(\tau)$. The calculations in Figure 2 employed the full expression for $\Gamma(t)$ in eq 13, but the results are very similar to those obtained by setting $\Gamma'' \rightarrow 0$.

The asymptotic time dependence of the echo signal at long times for a quantum solvent, depicted by the $Q = 200$ curve in Figure 2, may be deduced from the long-time limit of $\Gamma(t)$ in eq 13. An asymptotic expansion of $\zeta(t)$ in even powers of $1/t$ may be generated by successive integrations by parts of eq 16. This expansion may then be substituted into the time derivative of the expression for the real part of $\Gamma(t)$ in eq 13, $\dot{\Gamma}'(t)$, to yield an expansion of that quantity in odd powers of $1/t$. An exponential echo decay implies that $\dot{\Gamma}'(t)$ is independent of time,

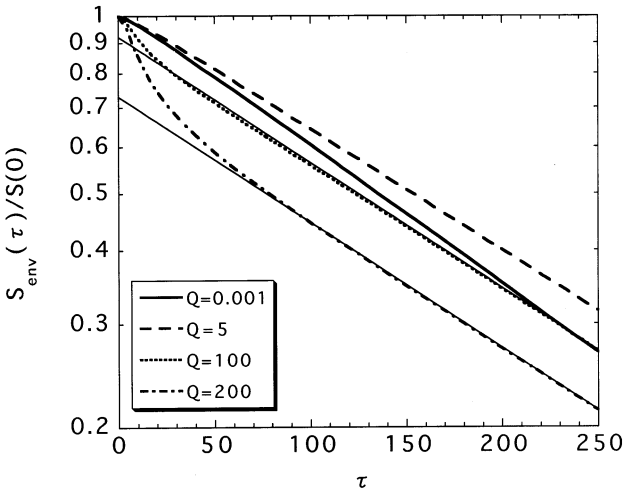

Figure 3. The crossover to the classical mechanical asymptotic long time decay of the vibrational echo signal $S(\tau)$ for a quantum system is shown. As in Figure 2, $F = 0.1$, $\lambda = 6\omega_0^{-1}$, and $\eta = m_0\omega_0$. $Q = 0.001$ (thick solid curve), $Q = 5$ (dashed curve), $Q = 100$ (dotted curve), and $Q = 200$ (dot−dash). Thin solid lines show the long-time limits of exponential decay for $Q = 100$ and $Q = 200$.

so that $\dot{\Gamma}'(t)$ has the physical significance of an instantaneous dephasing rate:

$$\dot{\Gamma}'(t) \approx T_2^{-1}[1 - \theta_1/t + (\theta_3/t)^3 + O(t^{-5})] \qquad (28)$$

$$\theta_1 = 2\lambda/\pi \qquad (29)$$

$$\theta_3 = \lambda[(2/3\pi)(1 + (\beta\hbar)^2/(2\lambda^2)]^{1/3} \qquad (30)$$

The long time limit of eq 28, T_2^{-1}, is constant, indicating an asymptotic exponential decay of the echo at long times. The decay constant is independent of $\hbar$, as is the t^{-1} correction which describes the approach to the long time exponential limit for both classical and quantum solvents. The largest correction to the long time limit of $\dot{\Gamma}'(t)$ containing $\hbar$ is the t^{-3} term in eq 28. In the long time limit for both classical and quantum solvents, the echo decay is exponential in time and controlled by the classical pure dephasing time T_2.[29] For the Ohmic spectral density employed here, at sufficiently long time, the echo observable will be dominated by interactions of the solute with solvent modes of sufficiently low frequency to be treated classically. In the strongly quantum regime in which both solute and solvent are quantum mechanical, the echo decay becomes classical for τ greater than a crossover time $t_x = \beta\hbar/6^{1/2}$ at which the t^{-1} and t^{-3} terms in eq 28 are comparable in magnitude. Figure 3 shows a semilogarithmic plot of the echo signal for $F = 0.1$, $\lambda = 6\omega_0^{-1}$, and $\eta = m_0\omega_0$ (as in Figure 2), with $Q = 0.001$ (thick solid), $Q = 5$ (long dash), $Q = 100$ (dots), and $Q = 200$ (dot−dash). Thin solid lines with slope $-2/T_2$ show the long-time asymptotic decays for $Q = 100$ and $Q = 200$, predicted in eq 28. Consistent with the preceding analysis, Figure 3 shows that the crossover to classical dephasing dynamics occurs at increasing values of τ for increasing Q. For $Q = 100$ and $Q = 200$, $t_x \approx 41\omega_0^{-1}$, and $t_x \approx 82\omega_0^{-1}$, respectively. Figure 3 shows that these times correspond to the crossover between short-time quantum dynamics and long-time classical dynamics. This analysis suggests that as Q is decreased, the echo decay in the motional narrowing limit will approach an exponential decay at decreasing values of τ. Indeed, for $Q = 5$ in Figure 3, this scenario appears valid. However, for $Q < 1$, the solute approaches the classical limit, and the echo signal reflects not only damping from the solvent, but solute dynamics, which are manifest in beats involving different transition frequencies in the Morse oscillator. For this reason, the calculation with $Q = 0.001$ does not resemble a pure exponential decay over the time scale of Figure 3.

We have considered quantum corrections to classical modeling of the vibrational echo from a solvated anharmonic oscillator. The theory is valid for a separation of time scales between a high-frequency solute and low-frequency solvent. In this case, the vibrational echo reflects the pure dephasing of the solute, and vibrational energy transfer between solute and solvent is neglected. For this separation of time scales, we can consider separately the effect of quantum corrections on solute and solvent dynamics. Quantum effects in solute and solvent dynamics must be considered when the frequencies of the relevant vibrations are comparable to or larger than $kT/\hbar$, a condition commonly met in molecular systems at room temperature or below. However, the relatively small magnitudes of quantum corrections to the vibrational echo from both solute and solvent dynamics shown in Figures 1−3 suggest that in the absence of significant vibrational energy transfer between solute and solvent, classical or semiclassical mechanical treatments can provide qualitatively correct descriptions of the nonlinear vibrational response of condensed phase molecular systems.

Acknowledgment. This research was supported by the National Science Foundation through Grant No. CHE0105623, and by the Petroleum Research Fund of the American Chemical Society. R.A. is a Research Fellow of the Japan Society for the Promotion of Science (2000). R.F.L. acknowledges 15 years' worth of thought-provoking discussions of nonlinear spectroscopy with Professor A. C. Albrecht.

References and Notes

(1) Mukamel, S.; Piryatinski, A.; Chernyak, V. *Acc. Chem. Res.* **1999**, *32*, 145.
(2) Fayer, M. D. *Annu. Rev. Phys. Chem.* **2001**, *52*, 315.
(3) Hamm, P.; Lim, M.; Hochstrasser, R. M. *Phys. Rev. Lett.* **1998**, *81*, 5326.
(4) Zanni, M. T.; Ge, N. H.; Kim, Y. S.; Decatur, S. M.; Hochstrasser, R. M. *Biophys. J.* **2002**, *82*, 66.
(5) Wright, J. C. *Int. Rev. Phys. Chem.* **2002**, *21*, 185.
(6) Golonzka, O.; Khalil, M.; Demirdoven, N.; Tokmakoff, A *J. Chem. Phys.* **2001**, *115*, 10814.
(7) Stenger, J.; Madsen, D.; Hamm, P.; Nibbering, E. T. J.; Elsaesser, T. *J. Phys. Chem A* **2002**, *106*, 2341.
(8) Merchant, K. A.; Thompson, D. E.; Xu, Q.-H.; Williams, R. B.; Loring, R. F.; Fayer, M. D. *Biophys. J.* **2002**, *82*, 3277.
(9) Merchant, K. A.; Noid, W. G.; Thompson, D. E.; Akiyama, R.; Loring, R. F.; Fayer, M. D. *J. Phys. Chem. B.* In press.
(10) Scheurer, C.; Piryatinski, A.; Mukamel, S. *J. Am. Chem. Soc.* **2001**, *123*, 3114.
(11) Keyes, T.; Fourkas, J. T. *J. Chem. Phys.* **2000**, *112*, 287.
(12) Saito, S.; Ohmine, I. *Phys. Rev. Lett.* **2002**, *88*, 207401.
(13) Ma, A.; Stratt, R. M.; *J. Chem. Phys.* **2002**, *116*, 4962.
(14) Mukamel, S.; Khidekel, V.; Chernyak, V. *Phys. Rev. E* **1996**, *53*, R1.
(15) Williams, R. B.; Loring, R. F. *J. Chem. Phys.* **2000**, *113*, 1932.
(16) Williams, R. B.; Loring, R. F. *Chem. Phys.* **2001**, *266*, 167.
(17) Akiyama, R.; Loring, R. F. *J. Chem. Phys.* **2002**, *116*, 4655.
(18) Wu, J.; Cao, J. *J. Chem. Phys.* **2001**, *115*, 538.
(19) Sage, M. *Chem. Phys.* **1978**, *35*, 375.
(20) Mukamel, S. *Principles of Nonlinear Spectroscopy*; Oxford University Press: New York, 1995.
(21) Sung, J. Y.; Silbey, R. J.; Cho, M. *J. Chem. Phys.* **2001**, *115*, 1422.
(22) Sung, J. Y.; Silbey, R. J.; *J. Chem. Phys.* **2001**, *115*, 9266.
(23) Suzuki, Y.; Tanimura, Y. *J. Chem. Phys.* **2001**, *115*, 2267.
(24) Suzuki, Y.; Tanimura, Y. *Chem. Phys. Lett.* **2002**, *358*, 51.
(25) Zwanzig, R. *J. Stat. Phys.* **1973**, *9*, 215.
(26) Klauder, J. R.; Anderson, P. W. *Phys. Rev.* **1962**, *125*, 912.
(27) Georgievskii, Y. I.; Stuchebrukhov, A. A.; *J. Chem. Phys.* **1990**, *93*, 6699.
(28) Kubo, R., in *Fluctuations, Relaxation, and Resonance in Magnetic Systems*; Plenum Press: New York, 1962.
(29) Oxtoby, D. W. *Adv. Chem. Phys.* **1979**, *40*, 1.
(30) Tuckerman, M.; Berne, B. J.; *J. Chem. Phys.* **1993**, *98*, 7301.